DETERMINING THE COHERENCE OF MICROPULSES

T. E. STROHMAYER,[1] J. M. CORDES,[2] AND H. M. VAN HORN[1]

ABSTRACT

The detection of coherent periodicities in pulsar signals would provide strong evidence for the presence of oscillations in neutron stars. To investigate the neutron star oscillation hypothesis further we have developed a technique, based on analysis of the Fourier cross spectra of high time resolution, single pulse data, that is useful for measuring the coherence properties of micropulses and for determining whether or not coherent periodicities may be present in some pulsars. We have used this technique to examine the coherence of micro-structure in PSR 2016+28. Our analysis of 2000 consecutive pulses recorded at 430 MHz and smoothed to 100 μs time resolution confirms the presence of quasi-periodic microstructure with period $P_\mu \approx 0.9$ ms in this pulsar. We also find that the coherence time of the quasi-periodicity is considerably shorter than one single rotation period for this object ($P = 0.53$ s), giving a $Q \approx 6$. By comparison with several numerical simulations of micropulse separation, we conclude that if the quasiperiodic separations are due to phase jitter of a coherent periodicity, the rms jitter must be $\geq 35\%$ of the micropulse period. Although the observed micropulse separations appear not to be coherent, the subpulse separation, $P_2 \approx 10$ ms, is coherent across several pulse periods. The degree of coherence is consistent with a model in which the average subpulse drift rate has a fixed, constant value, but in which individual subpulse drift rates exhibit random variations about that mean. For an average drift rate of 2 ms the data are consistent with an rms variation of 0.08 ms (4%), with a $Q \approx 90$. We discuss the status of the neutron star oscillation hypothesis in light of these new results.

Subject headings: pulsars: general — stars: neutron — stars: oscillations

1. INTRODUCTION

Neutron stars can sustain a variety of different oscillation modes (McDermott 1985; Strohmayer 1991). This diversity arises from the different restoring forces that act on a displaced mass element: gravity, pressure gradients, elastic forces in the crustal material, magnetic fields, and the Coriolis force in rotating neutron stars (pulsars). Observational identification of any of these oscillation modes would give astrophysicists a direct probe of the internal structure of neutron stars.

The detection of millisecond variability in PSR 2016+28 prompted Boriakoff (1976) and Van Horn (1980) to speculate that quasi-periodic variability in pulsars is a manifestation of oscillations of the underlying neutron star. Boriakoff (1976) suggested that pulsation-driven "shaking" of magnetic field lines "frozen" into the surface layers of the neutron star might modulate the pulsar emission process. Alternatively, a temperature perturbation induced by oscillations near the magnetic polar cap of the neutron star could modulate the plasma injection process, which powers the radio emission in some theoretical model of pulsars (Jones 1987).

At present it is not clear exactly how, or indeed if, oscillations of the underlying neutron star modulate the radio emission from pulsars. The existence of quasi-periodic microstructure in some pulsars is well established (Hankins 1971; Kardashev et al. 1978; Cordes 1979; Soglasnov et al. 1981; Cordes, Weisberg, & Hankins 1990), but the quasi-periodicities are typically observed to be low-Q phenomena. Many pulsars are known to display other varieties of temporal modulation. For example, Backer (1973) and Rankin (1986) have studied the drifting subpulses which are prominent in some pulsars. It has been suggested that the radio beam motion (see Arons 1981) is responsible for this phenomenon, but this may not explain all aspects of the problem. For example, the power spectrum of the intensity at fixed pulse phase indicates that the drift *bands* have poorly defined separations and are therefore not coherent in this pulsar (Backer 1973). Yet, our analysis of 430 MHz data from PSR 2016+28 indicates that the subpulse separation within individual pulses (P_2) is coherent across several pulses (see § 4), suggesting that a fairly high-Q process, such as stellar oscillation, might be responsible for the subpulse separations in individual pulses. We discuss this possibility in more detail in a later section.

The case for association of the observed temporal variations in pulsar data with neutron star oscillations would be greatly strengthened if it could be shown that any of the quasi-periodic variations were coherent across several individual pulses. Coherence times longer than one pulse period would lend strong support to the idea of a clock, such as stellar oscillation, underlying these variations. Alternatively, processes in the pulsar magnetosphere may be responsible for the quasi-periodicities, as recently proposed in a plasma model by Asseo, Pelletier, & Sol (1990). In this case neutron star oscillations may manifest their presence in some other way, or perhaps not at all, in the radio emission. In either case, measurement of the micropulse coherence time provides useful information about the mechanism responsible for the quasi-periodic microstructure.

In this paper we attempt to address some of these questions in order to explore more completely the neutron star oscillation hypothesis in the context of a single pulsar. We have chosen to investigate PSR 2016+28 because a high percentage of its pulses show quasi-periodic microstructure. This pulsar also exhibits drifting subpulses, does not null, and is otherwise

---

[1] Department of Physics and Astronomy, University of Rochester, Rochester, NY 14627-0011.

[2] Astronomy Department, Cornell University, Space Science Building, Ithaca, NY 14853-6801.

well studied, making it an excellent candidate for this analysis. Throughout this work we have relied extensively on numerical simulations to provide us with a precise understanding of the analysis techniques we have employed, as well as to help us interpret the results. To avoid biasing ourselves toward any one theoretical scenario, we have endeavored to include a wide range of possibilities in our analyses and simulations.

In § 2 we describe the techniques we have used to search for coherent periodicities and to measure the coherence properties of micropulses in pulsar signals. We discuss our pulsar simulations in § 3. In § 4 we discuss our analysis of 430 MHz, single pulse data from PSR 2016+28. Our conclusions are summarized in § 5.

2. ANALYSIS TECHNIQUES

As is common in the analyses of time series, we use Fourier transform techniques to search for coherent periodicities in pulsar signals. Since oscillations in neutron stars can occur with periods smaller than tenths of milliseconds (McDermott, Van Horn, & Hansen 1988; Strohmayer 1991) it is important to examine data with high time resolution. Our 430 MHz data set from PSR 2016+28 was sampled at 100 μs time intervals (Thorsett 1990). A typical data set consists of a train of N_p consecutive pulses, each containing K data samples taken in a narrow window centered on the mean pulse profile. The Fourier transform of each pulse is computed using a fast Fourier transform (FFT) algorithm (Press et al. 1986). The individual pulse transforms are then used to compute the *auto spectrum* and the *cross spectrum* for the entire set of pulses. The auto spectrum is simply the average power spectrum,

$$A(f) = \frac{1}{N_p} \sum_{i=1}^{N_p} P_i^*(f) P_i(f) , \qquad (2.1)$$

where $P_i(f)$ is the Fourier transform of pulse i. The cross spectrum is defined as

$$
\begin{aligned}
&C_l(f) \exp\left[i\phi_l(f)\right] \\
&= \frac{\sum_{i=1}^{N_p-l} P_{i+l}^*(f) P_i(f)}{\left[\sum_{i=l+1}^{N_p} P_i^*(f) P_i(f) \sum_{i=1}^{N_p-l} P_i^*(f) P_i(f)\right]^{1/2}} .
\end{aligned} \qquad (2.2)
$$

In equation (2.2) $C_l(f)$ and $\phi_l(f)$ represent the amplitude and phase, respectively, of the cross spectrum. The quantity l is the *lag* in number of pulses, and an asterisk denotes complex conjugation. From the Fourier convolution theorem, the cross spectrum in frequency space is closely related to the cross-correlation function in the time domain. We can thus correlate the data at lags given by an integer number of pulse periods, lP, thereby determining the coherence properties of the signal. For example, if a strictly periodic signal is present throughout an entire sample of pulses then the amplitude of the cross spectrum at that frequency is close to unity and independent of l, and the phase of the cross spectrum increases linearly with l. Alternatively, if the amplitude of a periodic signal decays with some characteristic time scale (longer than a pulse period, say) over the entire data set, then the amplitude of the cross spectrum decays with l in an analogous fashion (this behavior is clearly seen in many of our simulations). If no periodic signals are present (as with the purely random simulations we have performed), then the cross spectrum approaches zero as we average more pulses. As indicated in equation (2.2) we have chosen to normalize the cross spectrum to unit amplitude. Thus, cross spectral amplitudes near unity indicate strong coherence, whereas smaller amplitudes specify weak coherence.

Many previous studies (Hankins 1971; Boriakoff 1976; Cordes et al. 1990) have employed the intensity autocorrelation function (ACF) and the intensity cross correlation function (CCF) in examining pulsar microstructure. Since we are interested in examining the coherence properties of microstructure in specific frequency regimes (i.e., at frequencies which correspond to the quasi-periodic micropulses), as well as in searching for high-Q periodicities we find it more convenient to work in the frequency domain.

3. ANALYSIS OF SIMULATED PULSAR SIGNALS

In order to test our analysis techniques and estimate the level at which periodic signals may be present in pulsar data we have conducted a series of numerical experiments using simulated pulsar signals. We have used the techniques described above to examine the power spectra, the auto spectra and the cross spectra of these signals. In developing these simulated pulsar signals we have been guided by two basic precepts: (1) Start with simple models and add sophistications as the simple models are understood. (2) Examine both fully random and completely deterministic models. We emphasize that in generating these simulations our goal has *not* been to attempt to model precisely the signals from individual pulsars, but rather to test our ability to diagnose signals having specific properties. In the remainder of this section we describe these models in some detail, and we discuss the results of simulations conducted with them.

3.1. *Simple Deterministic Signals*

To test our techniques and computing codes we have examined spectra of deterministic signals of the general form

$$
S(t) = \Theta(t)\left\{ W(t)\left[A_0 + \sum_{i=1}^{M} A_i \cos\left(2\pi\nu_i t + \phi_i\right) \right] + N(\sigma_n) \right\} ,
$$

$$(3.1.1)$$

where A_i, ν_i, and ϕ_i are the amplitude, frequency, and phase, respectively, of M strictly periodic components. The quantity $N(\sigma_n)$ is a zero-mean Gaussian noise process with standard deviation σ_n, and $\Theta(t)$ is a periodic function (with period equal to the pulsar spin period) that defines the "observing" window around the mean pulse profile. The function $W(t)$ is a waveform which is meant to simulate the mean pulse profile of the pulsar. In all of our simulations we model the mean pulse profile as a sum of Gaussian components. When the average pulse waveform $W(t)$, is constant (independent of t) the power spectrum of this signal can be calculated analytically. Results from such signals can thus be used to test the accuracy of our numerical calculations. For all signals of this type, our numerical results are entirely consistent with the analytic formulae. Figure 1 shows a typical auto spectrum computed from such a model (with parameters given in the figure caption). This realization contained three distinct periodic components, each with a different amplitude. The amplitude $C_l(f)$ and phase $\phi_l(f)$ of the cross spectrum, plotted as a function of lag are shown in the inset panels. In this case the cross spectrum was evaluated at the center frequency of the strongest periodicity (bin 93). This simulation clearly displays the features of coherent signals: (1) the amplitude of the auto spectrum peaks at the frequencies of any strictly periodic signals; (2) the amplitude of the cross spectrum at the frequency of a strictly periodic signal is independent of the lag, l; and (3) the phase of the cross spectrum increases linearly with l. In this case the phase of the cross spectrum is constant because the spin period and the oscillation period, $\Pi_1 = 1/\nu$, were chosen to be commensurate.
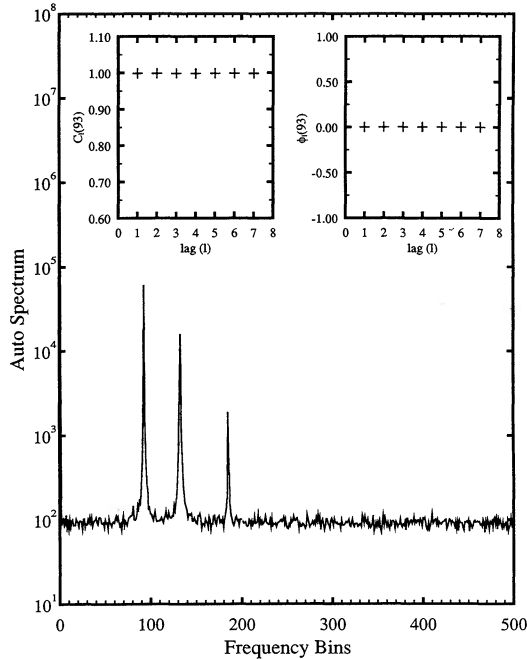
FIG. 1.—Plot of the auto spectrum computed from a set of 100 pulses generated with the deterministic model of eq. (3.1.1). In this realization we generated 1024 samples per pulse with a time resolution $\delta = 90$ μs. The model parameters are: $A_0 = 1$, $A_1 = 0.5$, $A_2 = 0.3$, $A_3 = 0.1$, $\Pi_1 = 1.0$ ms, $\Pi_2 = 0.7$ ms, $\Pi_3 = 0.5$ ms, and $\phi_i = 0$. The standard deviation of the gaussian noise process, σ_n, is 0.3. The frequency in Hz is given by the expression $f = $ (bin No./512) $\times f_{Nyq}$, where $f_{Nyq} = 1/(2\delta)$ is the Nyquist frequency. The inset panels, from left to right, show the amplitude and phase of the cross spectrum plotted as a function of lag. The cross spectrum is evaluated at bin 93, the center frequency corresponding to Π_1.

In another experiment with this model, we introduced an exponential time decay of the amplitude of the first periodic component. The decay in the amplitude of the cross spectrum as a function of lag l centered at this periodicity is clearly seen in the left inset of Figure 2, where the auto spectrum and the cross spectrum are displayed as in Figure 1. The reduced intensity of the first periodic signal, centered at bin 93, is also clearly seen in the auto spectrum. In this case the decay time was equal to one pulse period. Comparison of real data with results from this experiment would allow us to estimate decay times of oscillations, if modes such as these were found to be present in actual data.

3.2. *Simulated Pulsar Signals*

In addition to the purely deterministic signals discussed above, we also find it useful to explore the properties of simulations that more accurately characterize the true nature of the pulsar signals. For this purpose we use a shot-noise model to simulate pulsar emission. Such models are quite similar to the amplitude-modulated noise model (AMN) discussed by Rickett (1975) and Cordes (1976b), which can account for many of the properties of observed pulsar signals. Our simplest, *one-component*, shot-noise model generates Gaussian shots with random amplitudes, which are distributed in time according to Poisson statistics, and is of the form

$$S(t) = \Theta(t)\{W(t)[G(\mu_s, \eta_s)] + N(\sigma_n)\} . \qquad (3.2.1)$$

The Gaussian pulses $G(\mu_s, \eta_s)$ are characterized by a fixed width in time (standard deviation) μ_s, and a mean time separa-
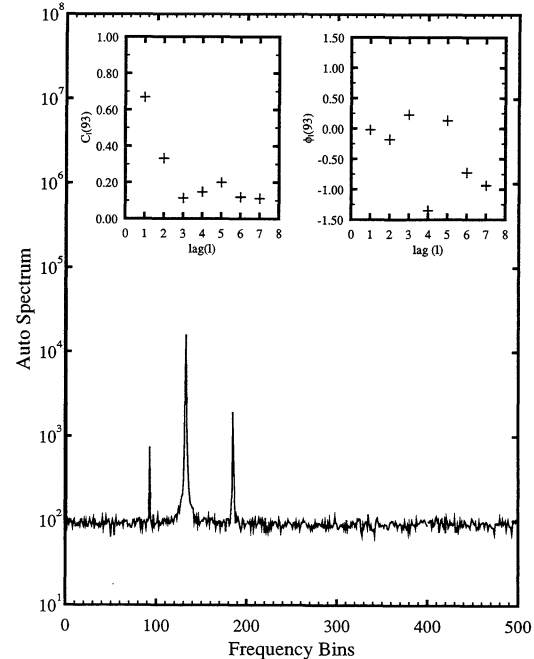

FIG. 2.—Auto spectrum of the same model as shown in Fig. 1 except that the amplitude A_1 is given by $A_1(t) = A_1 e^{-t/\tau}$ with $\tau = 1$ pulsar spin period. The inset panels, from left to right, show the amplitude and phase of the cross spectrum plotted as a function of lag. The cross spectrum is evaluated at bin 93, the center frequency corresponding to Π_1. Notice the decrease in the cross spectral amplitude with lag.

tion η_s. Zero-mean Gaussian noise with standard deviation of the amplitude given by σ_n is included to model the noise present in any detector system. The random amplitudes of the Gaussian shots are drawn either from a uniform distribution with some maximum amplitude, or from a Gaussian distribution with mean A_s and standard deviation B_s. The other symbols have the same meanings as in equation (3.1.1). To construct the individual pulses a random number code generates the location in time of successive shot centroids. The code uses successive centroid locations, two at a time, to compute the signal strength at uniformly spaced intervals within each pulse window.

This simple model provides an adequate characterization of the longer time (5–10 ms) features seen in real pulsar signals. For example, Figure 3a shows a plot of 10 consecutive pulses taken from a total of 200 which were generated with this model. In Figure 3b we have plotted the auto spectrum and the cross spectrum, $C_1(f)$, computed from the entire sample of 200 pulses. The model parameters are given in the caption of Figure 3a. The prominent peak centered at zero frequency in the auto spectrum is due to the Gaussian shots. This feature is common to all of our one-component simulations. The width in frequency of the peak in the auto spectrum is inversely proportional to the shot width, μ_s. The high-frequency end of the spectrum is asymptotically flat, consistent with the contribution from the Gaussian noise component. The magnitude of the cross spectrum, $C_1(f)$, for this realization is shown in the inset of Figure 3b. The solid line through the spectrum is the mean value across the entire frequency range, and the dashed line is the corresponding 3 σ level. For this fully random model the deviation of the cross spectrum for noise is zero to within the limits introduced by averaging a finite train of pulses. This
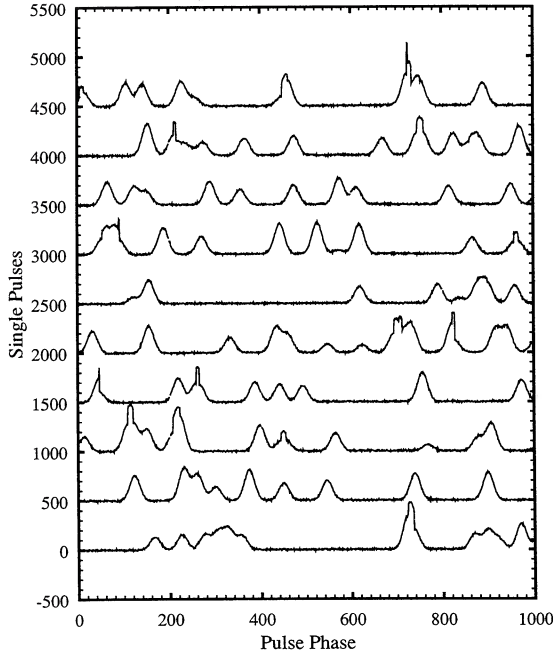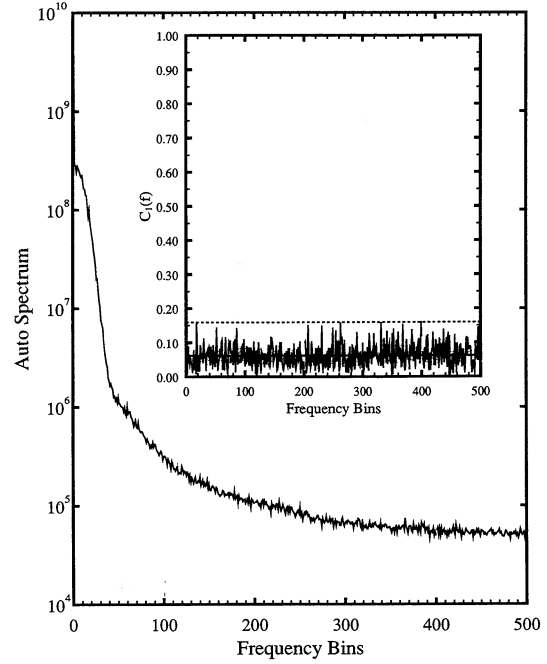
FIG. 3a

FIG. 3b

FIG. 3.—(a) Sample of 10 consecutive pulses generated with the one-component shot-noise model of eq. (3.2.1). A total of 1024 points per pulse were sampled with 90 μs time resolution. The model parameters were $\mu_s = 1.0$ ms, $\eta_s = 8.0$ ms, and $\sigma_n = 5.0$. The amplitudes of the Gaussian pulses were drawn from a Gaussian distribution with mean amplitude $A_s = 200.0$, and standard deviation $B_s = 70.0$. Time increases upward, to the right. For clarity, each successive pulse is displaced upwards by 500.0 from the previous pulse. (b) Auto spectrum computed from a sample of 200 pulses generated with the one-component shot-noise model of Fig. 3a. The Gaussian-like peak near zero frequency is characteristic of the one-component models. The width of the peak is inversely proportional to the shot width, μ_s. The inset panel shows the amplitude of the cross spectrum $C_1(f)$. The solid line denotes the mean value of the cross spectrum. The dashed line is the corresponding 3 σ value.

is as expected, since the signal was constructed to be purely random.

In order to make the shot-noise model described above more realistic, we next incorporated, approximately, the effects of an average pulse profile on the simulated signals. This was done by applying a profile modulation function, $W(t)$, as in equation (3.1.1), to the Gaussian shots G in equation (3.2.1). Thus, the random signals generated as described above are multiplied at each time interval by the value of a profile function appropriate to that position in the pulse window. As we are specifically interested here in PSR 2016+28 we have chosen parameters specifically to simulate pulses from this pulsar. The techniques are generally applicable, however, and we have employed such models successfully in other cases as well. Since PSR 2016+28 also has drifting subpulses we have chosen to model the average profile as the product of two components; an overall Gaussian mean profile, and a drifting subpulse envelope. The mean pulse component is fixed in time with respect to the observing window and is characterized by a width, σ_w. The subpulse envelope is composed of Gaussian components of width, σ_{sp}, whose centroids are separated by an amount, Δ. The subpulse envelope drifts through the observing window by a specified amount, t_d, in each pulse period. We have also permitted random variations with standard deviation σ_d around this mean drift rate. In computing these simulations we have attempted to adopt parameters which are consistent with our actual 430 MHz data set from PSR 2016+28, but we emphasize we have not done any precise fitting of the parameters.

We are also interested in studying micropulse properties as well as subpulses. We must therefore extend the shot-noise

models to simulate the shorter time scale *micropulse* emission as well as the subpulse emission. As before, the micropulses are simulated as Gaussian shots. In this *two-component* model we allow the subpulse and micropulse widths to have some variation about their respective mean values. Thus, each component is specified by two parameters, the mean component width, μ, and the variation about that mean, σ. The subpulse parameters are noted by μ_s, and σ_s, while the micropulse parameters are μ_m, and σ_m. The signal of the two-component model is of the form

$$S(t) = \Theta(t)\{W(\sigma_w, \sigma_{sp}, \Delta, t_d, \sigma_d, t)[G_1(\mu_s, \sigma_s, \eta_s) + G_2(\mu_m, \sigma_m, \eta_m)] + N(\sigma_n)\} . \qquad (3.2.2)$$

Here $G_1(\mu_s, \sigma_s, \eta_s)$ represents the subpulse component and $G_2(\mu_m, \sigma_m, \eta_m)$ the micropulse component. The mean profile function $W(\sigma_w, \sigma_{sp}, \Delta, t_d, \sigma_d, t)$ is described in the preceding paragraph. In these more realistic models the time separations between adjacent subpulse centroids and between adjacent micropulse centroids are also given by Poisson distributions with fixed means η_s, and η_m. However, the amplitudes of the subpulses and micropulses are drawn from two distinct Gaussian distributions. Variations of the means and standard deviations of these distributions allow us to increase or decrease the relative strength of either the micropulse or subpulse components in these signals.

We illustrate the types of signals that can be generated using this model with several examples. In Figure 4 we have plotted a sequence of 10 consecutive pulses generated with the model described above (*right panel*) together with a sequence of 10 pulses actually observed from PSR 2016+28 (*left panel*). The
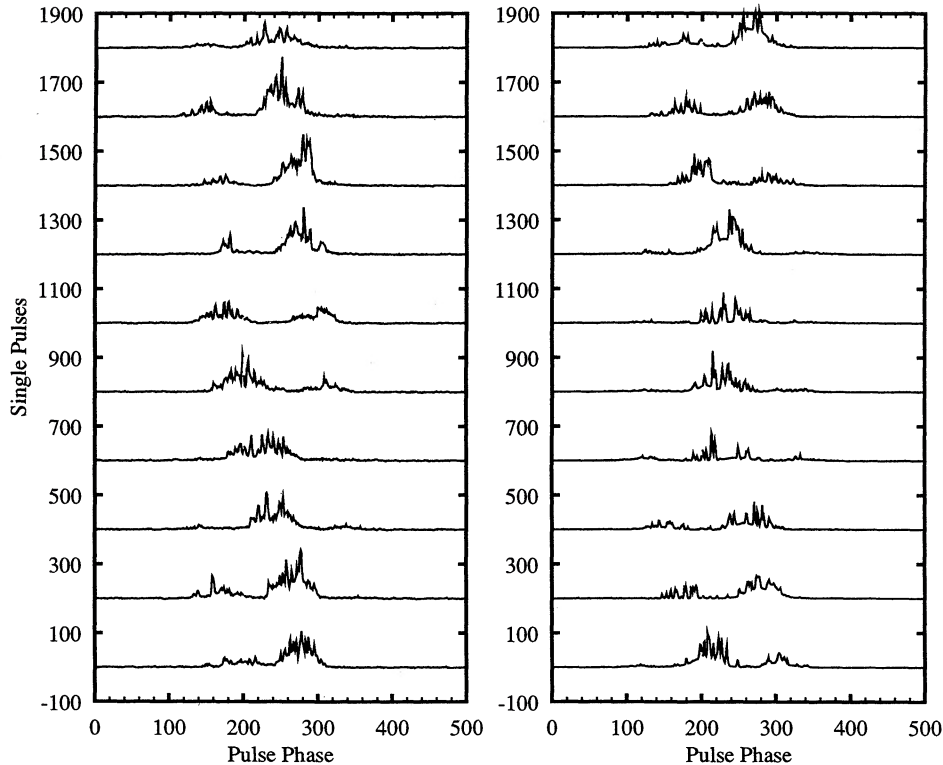
FIG. 4a

FIG. 4b

FIG. 4.—Sample of 10 consecutive pulses recorded at 430 MHz from PSR 2016+28 is shown in panel (a). Panel (b) shows a sample of 10 consecutive pulses generated with the two-component shot-noise model of PSR 2016+28. The model parameters used for this simulation are discussed in the text, and displayed in Table 1. Time increases upward, to the right, and each successive pulse is displaced upwards by 200.0 from the previous pulse.

values of the parameters used in this simulation are listed in Table 1. We have examined models with a constant subpulse drift rate as well as models where the drift rate is variable about some mean value. The pulses displayed in Figure 4 were generated with the variable drift rate model. For convenience we have constrained the drifting subpulse envelope in the constant drift rate simulation to appear at the same position in pulse phase every 6 pulse period. We find that both of these

models are able to reproduce much of the structure seen in the actual 430 MHz data. In Figure 4 notice that the microstructure appears as additional substructure of the individual subpulses, as discussed by Cordes et al. (1990). The auto spectrum of this 500 pulse simulation is displayed in Figure 5, as is the magnitude of the cross spectrum $C_1(f)$ (inset).

There are several noteworthy features of this spectrum: (1) The narrow Gaussian peak near zero frequency is familiar

TABLE 1

PARAMETERS USED IN PULSAR SIMULATIONS

Parameter	Two-component shot-noise model	Description
Parameters of Random Signal		
$\mu_s(\sigma_s)$ (ms)	2.0(0.1)	mean(deviation) of subpulses
$\mu_m(\sigma_m)$ (μs)	100.0(20.0)	mean(deviation) of micropulses
η_s (ms)	4.0	mean separation between subpulses
η_m (μs)	350.0	mean separation between micropulses
$A_s(B_s)$	30.0(5.0)	amplitude(deviation) of subpulses
$A_m(B_m)$	45.0(20.0)	amplitude(deviation) of micropulses
σ_n	0.15	deviation of noise component
Parameters of Mean Profile Function		
σ_w (ms)	5.0	width of mean pulse
σ_{sp} (ms)	2.2	width of individual subpulses
Δ (ms)	12.0	separation between subpulse centroids
$t_d(\sigma_d)$ (ms)	2.0(0.08)	mean(deviation) subpulse drift rate
δ (μs)	100.0	time between samples

NOTES.—Values of the parameters used in the two-component pulsar model. The third column gives a brief explanation of each parameter. See § 3.2 for a detailed description of the model parameters.
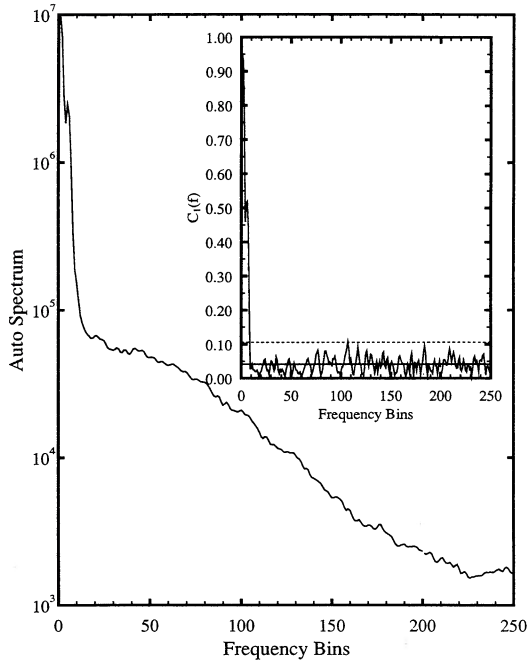
FIG. 5.—Auto spectrum and the cross spectrum $C_1(f)$ (amplitude) computed from a set of 500 pulses generated with the two-component shot-noise model of PSR 2016+28 are plotted as a function of frequency. The model parameters used for this simulation are given in Table 1. The subpulse separation feature is centered on bin 6 in both the auto and cross spectrum.

from the one-component model, but now we also see a broad feature extended to higher frequencies. This is due to the narrow micropulses. (2) There is a clear feature seen in the low-frequency component of the spectrum at bin 6. The location of this feature measures the separation between subpulses and corresponds to the parameter P_2 used to characterize drifting subpulses in pulsars. We have confirmed this identification by examining the position of the feature as a function of the subpulse separation Δ in our subpulse envelope model. (3) The cross spectrum, $C_1(f)$, shows a strong signal at the subpulse separation feature (bin 6), while the remainder of the spectrum is essentially zero, consistent with the random nature of the micropulses.

Comparison of the spectra computed from these simulated pulses with the spectra obtained from our 430 MHz PSR 2016+28 (see below) data indicates that our two-component, shot-noise model is quite suitable as a null hypothesis; that is, the presence or absence of periodic signals in real pulsar data can be tested against a fully random shot-noise model. To quantify this procedure we compute the mean of the cross spectrum for one of our simulated signals. For our random, two-component shot-noise models the cross spectrum approaches zero as we average more pulses. That is,

$$\mu_C \propto (1/\sqrt{N_p}) , \qquad (3.1)$$

where μ_C is the mean of the frequency-averaged cross spectrum, and N_p is the number of pulses in the average. Real signals that show cross spectral amplitudes significantly higher than the mean level, μ_C, of one of our random simulations are thus candidates for signals containing coherent periodicities. The significance of a feature can thus be estimated by comparison with the mean and standard deviation of the local background.

4. ANALYSIS OF 430 MHz DATA FROM PSR 2016+28

Our data set consists of a sample of 2000 consecutive pulses from PSR 2016+28. The data were obtained at the Arecibo observatory with the 430 MHz feed and receiver system (Thorsett & Stinebring 1992). The pulses have been dedispersed and smoothed to a resolution of 100 μs. A total of 512 points was sampled in a 50 ms window centered on each pulse. A contaminating 60 Hz signal which had been picked up by the electronics during the data taking was subtracted from the data. This was accomplished by fitting a 60 Hz sinusoid to the off-pulse baselines (Thorsett 1990). We discuss the problem of interference and signal contamination in more detail in a later subsection.

As mentioned previously, Figure 4 (left panel) shows a sample of 10 consecutive pulses from this data set. Both the highly organized drifting subpulses in this group of pulses, as well as the strong micropulses are clearly apparent. Notice that the micropulses appear to be quasi-periodic in many individual subpulses.

In Figure 6 we have plotted the intensity integrated over the entire pulse window for each pulse in the data set. The main portion of the figure shows the integrated intensity plotted as a function of pulse number. The gradual decline in the integrated intensity towards the end of the data set is a result of interstellar scintillation. The inset panel shows the histogram of the integrated intensity, i.e., the number of pulses with an integrated intensity in each specified range. This distribution is rather sharply peaked, indicating that PSR 2016+28 is not an erratic emitter, and in fact does not show null pulses. To determine whether the data contain any significant long-term periodicities we have computed the power spectrum from the time series of the integrated intensities. The spectrum is flat, consistent with purely random variations of the intensity from pulse to pulse.
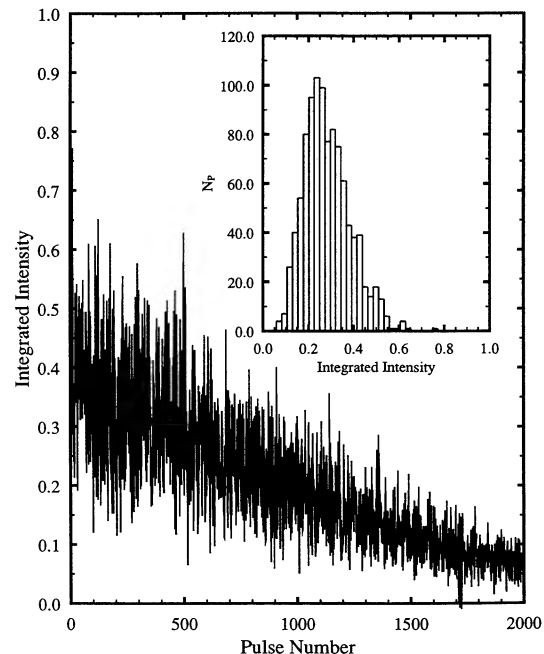

FIG. 6.—Plot of the intensity integrated over the pulse window as a function of pulse number. The decrease in pulse intensity is due to interstellar scintillation. The inset panel shows the histogram of the intensity integrated over the pulse window.

4.1. *Spectral Analysis*

To investigate the possibility that periodicities might be present only in a portion of the entire data set or that periodicities might occur only in certain ranges of pulsar luminosity, we have examined average spectra of various subsets of the entire sample. Since the integrated pulse intensity drops throughout the sequence of pulses, the first half of the data set has a higher signal-to-noise ratio than the second half. We therefore choose to display results from the first half of the data
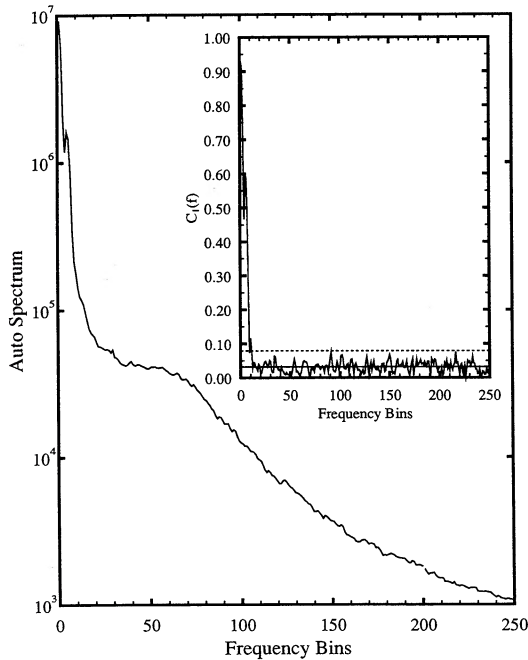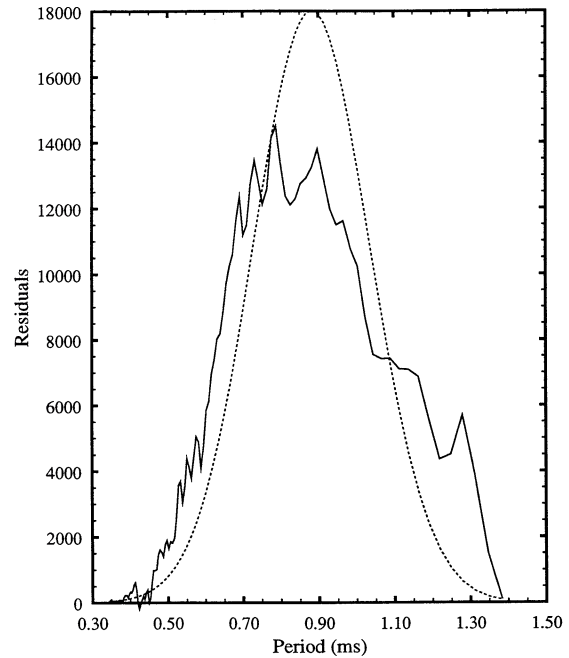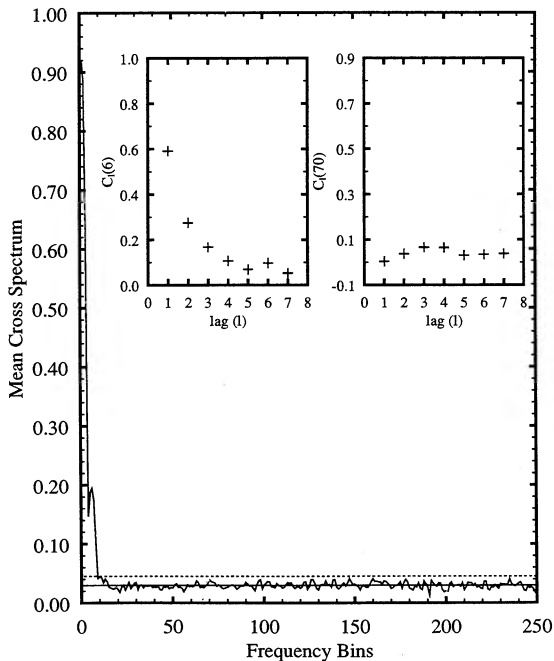
set. Because the pulses each contain 512 real-valued samples, the corresponding Fourier transforms contain information at only 256 positive frequencies. The relation between bin number and frequency in Hz is given by $f(\text{Hz}) = (\text{bin no.}/256) \times f_{\text{Nyq}}$, where $f_{\text{Nyq}} = 5000$ Hz for a 100 μs sampling rate.

Figure 7a shows the auto spectrum and the magnitude of the cross spectrum $C_1(f)$ (in the inset) of the first 1000 pulses. The auto spectrum displays the familiar subpulse-width peak centered at zero frequency, as well as a much broader component that extends to higher frequencies. The broad hump centered

FIG. 7a

FIG. 7b

FIG. 7c

FIG. 7.—(a) Auto spectrum computed from the first 1000 pulses of our data set from PSR 2016+28, is plotted as a function of frequency. Notice the subpulse separation feature centered on bin 6 and the broad micropulse quasi-periodicity feature centered near bin 70. The inset panel shows the cross spectral amplitude $C_1(f)$ plotted as a function of frequency. In this plot the solid line denotes the mean value in the frequency range from bin 50 to bin 250. The dashed line is the corresponding 3 σ level in the same frequency range. There is no evidence for coherence in the quasi-periodicity feature around bin 70 (see Fig. 8a for comparison with the two-component shot-noise model). (b) Residuals computed by subtracting a linear background from the auto spectrum of Fig. 7a are plotted as a function of period. The dashed curve is the best-fit Gaussian. The parameters of this Gaussian are given in § 4.1. (c) Mean of the $l = 1$–10 cross spectra computed from the first 1000 pulses of our data set from PSR 2016+28 is shown as a function of frequency. The solid line denotes the mean value in the frequency range from bin 50 to bin 250. The dashed line is the corresponding 3 σ value in the same frequency range. The left inset panel displays the amplitude of the cross spectrum evaluated at the subpulse separation feature (bin 6), as a function of lag. The drop in coherence over 4–5 pulse periods is evident. For comparison, the right panel shows the same quantity but now evaluated at the center of the micropulse quasi-periodicity feature (bin 70).

near bin 70 is the micropulse quasi-periodicity feature first detected by Boriakoff (1976) using the ACF. The feature corresponds to preferred micropulse separations of about 0.8–0.9 ms. The cross spectrum is essentially zero at the position of the micropulse quasi-periodicity feature, indicating that the micropulses are *not* coherent on a time scale longer than the pulsar spin period.

To estimate the Q-value of the micropulses we fit a linear function to the auto spectrum in the regions, bin 30–40, and bin 120–140. This provides a simple estimate of the background in the region of the micropulse feature. We then subtract this estimated background from the auto spectrum across the micropulse feature from bin 30 to bin 140. A plot of the residuals thus computed is shown in Figure 7b as a function of period, along with the best-fit Gaussian $Ae^{-(P-P_\mu)^2/2\sigma_\mu^2}$, where $A = 18021.24$, $P_\mu = 0.883$ ms, and $\sigma_\mu = 0.154$ ms. This procedure yields a Q-value for the micropulses of $Q \equiv P_\mu/\sigma_\mu = 5.7$. These results for the micropulse quasi-period, P_μ, and Q-value are entirely consistent with those orginally given by Boriakoff (1976).

To investigate the properties of the micropulses further we have introduced quasi-periodic micropulse separations into our shot-noise simulations. We have developed two distinct models for the micropulse separations. In the *coherent* model the micropulse centroids undergo a random variation about a set of strictly periodic recurrence times; such a model might be appropriate if there were an underlying clock mechanism for the quasi-periodicities. In this model we specify the coherent micropulse period, P_μ, and a standard deviation, σ_P, which is expressed as a percentage of the period. Note that we have used a value of $P_\mu = 0.8$ ms in these simulations to facilitate direct comparison with the data from PSR 2016+28. With this model we have analyzed a series of simulations generated by varying the deviation, σ_P, from 0% to 50%, while holding all other parameters fixed. In each case we record the strength of the coherent signal seen in the cross spectrum at the micropulse period, P_μ. The amplitude of the cross spectrum at the micropulse period drops from a high of ≈ 1 when $\sigma_P = 0\%$ to about 0.1 (the level of detection) for $\sigma_P = 35\%$. By comparison with this coherent model we can state that if the micropulse quasi-periodicities are produced by an underlying, coherent clock mechanism with some weak coupling to the magnetosphere, then the percentage jitter must be $\geq 35\%$ of the micropulse periodicity.

In our second model of micropulse separations the position in time of the centroid of a micropulse is referred only to the position of the previous micropulse. In this *random walk* model, the time separation of the micropulses is drawn from a Gaussian distribution with mean P_{rw} and standard deviation σ_{rw}. Using this model we have also investigated the loss of coherence as the standard deviation is increased from zero. In this case we find that the coherence level in $C_1(P_{rw})$ is undetectable when the standard deviation is $\approx 3\%$ of the micropulse quasi-period, for a micropulse quasi-period of 0.8 ms. This is consistent with the random walk interpretation, since phase loss will certainly occur after the micropulse centroids have "walked" a distance equal to at least one micropulse period. This will occur after a total of $N \approx 1/\epsilon^2$ steps, where ϵ is the standard deviation of the micropulse quasi-period expressed as a fraction of the quasi-period. When $\epsilon = 0.03$ (3.0%) the micropulse centroids can undergo $N \approx 1111$ steps before the phase is completely lost. This corresponds to less than 2 pulse periods, and therefore one would not expect to see

a coherent signature in the cross spectrum of this model. Interestingly, the auto spectrum of this model shows a strong spike at the micropulse period even when the standard deviation is as high as 25%. Since such a strong feature is clearly *not* seen in the auto spectrum of PSR 2016+28 we can conclude that if such a model were appropriate the deviation of the micropulse separations from strict periodicity would at least have to be greater than 25%.

The subpulse separation feature is also clearly seen in Figure 7a, centered near bin 6. This location corresponds to a subpulse separation of ≈ 10 ms, which is consistent with results obtained by Cordes et al. (1990) using the intensity ACF. This feature does show significant coherence. To investigate this further we have plotted in Figure 7c the mean of the $l = 1$–10 cross spectra. The mean cross spectrum simply averages out the noncoherent frequency components. The lack of coherence in the micropulse quasi-periodicity feature is even more appearent here than in Figure 7a, as the spectrum is essentially zero beyond bin 15. The two inset panels show the magnitude of the cross spectrum plotted as a function of lag for two different frequencies. The left panel shows the magnitude of the cross spectrum evaluated at the subpulse separation feature (bin 6). A fit to an exponential gives a characteristic decay time of $1.7P$. This corresponds to a Q-value by $Q \equiv$ (decay time)/(period) $= 1.7 \times 0.53$ s/10 ms ≈ 90. The right panel shows the same quantity but now evaluated at bin 70, the centroid of the micropulse quasi-periodicity feature. This confirms the previous result: there is no detectable coherence in the micropulse feature on time scales longer than a pulse period.

To enable the reader to make direct comparisons with results from a known signal we have computed the same quantities for a 1000 pulse shot-noise simulation using our two-component shot-noise model and a variable subpulse drift rate. The parameters used in computing this simulation are the same as those used in generating Figures 4 and 5, and are listed in Table 1. The results are displayed in Figures 8a and 8b. Notice that the magnitudes of the cross spectra obtained from the simulation are entirely consistent with those obtained from PSR 2016+28. In Figure 8b we show the mean computed from the $l = 1$–10 cross spectra. The left inset panel shows the cross spectral amplitude evaluated at the subpulse separation feature plotted as a function of lag. Notice the drop-off of the coherence as a function of lag. This is quite similar to what is seen in the cross spectrum of PSR 2016+28 (see Figs. 7a and 7b). This effect is a direct result of the variable subpulse drift rate used in this simulation. Similar calculations with a constant drift rate show a constant cross spectral amplitude as a function of lag. In this case an average drift rate of 2.0 ms with a standard deviation of 0.08 ms produces the cross spectral decay similar to that seen in PSR 2016 + 28. See Figures 7a and 7b for the corresponding data from PSR 2016+28.

4.2. *Problems with Interference*

As mentioned previously, a 60 Hz signal was removed from the data prior to our analysis using a simple fitting procedure applied to the off-pulse baselines. Through the course of our spectral analysis we discovered that the data were nevertheless still contaminated with higher harmonics of the fundamental 60 Hz interference. It is not clear whether these additional harmonics were an artifact of the 60 Hz filtering procedure, or were also present prior to that processing. We detected the contamination through analysis of the last 250 pulses of the sample. These pulses were significantly weaker than the
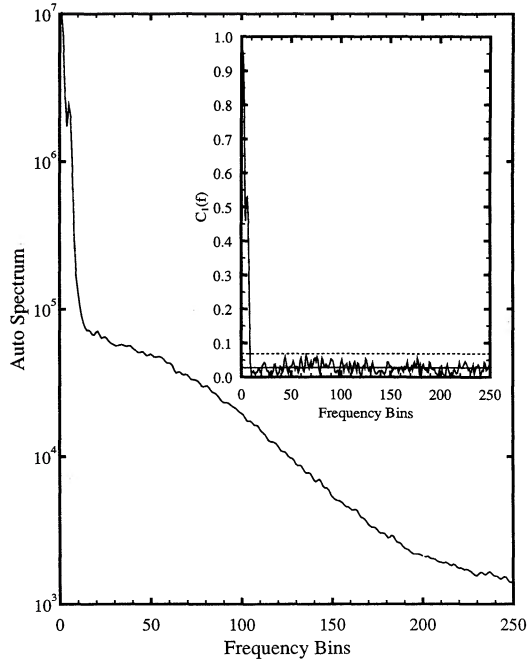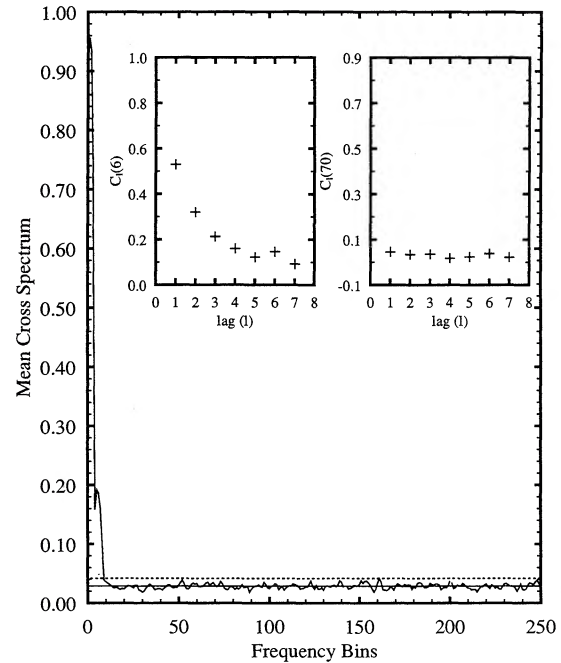
FIG. 8a

FIG. 8b

FIG. 8.—(a) Plot of the auto spectrum computed from the 1000 pulse, two-component, shot-noise model of PSR 2016+28. Details of the model are listed in Table 1. The inset panel shows the cross spectral amplitude $C_1(f)$ plotted as a function of frequency. Fig. 7a shows the corresponding results for PSR 2016+28. (b) Mean of the $l = 1$–10 cross spectra computed from the 1000 pulse, two-component, shot-noise model of PSR 2016+28 is plotted as a function of frequency. The left inset panel shows the cross spectral amplitude plotted as a function of lag. The cross spectrum was evaluated at the subpulse separation feature (bin 6). The right panel shows the same quantity but now evaluated at bin 70. Fig. 7b shows the corresponding results for PSR 2016+28.

average, because the pulsar was entering a scintillation minimum during this portion of the data acquisition (see Fig. 6), and the decline in the pulsar signal strength made it possible to detect the contaminating signals. In Figure 9 we show a plot of the mean cross spectrum ($l = 1$–10) calculated from the last 250 pulses in our sample. The strong contaminating signals are easily seen above the background. From left to right the strongest peaks correspond to the third, fifth, seventh, and fifteenth harmonics of the 60 Hz signal. By analyzing the spectra of portions of the off-pulse baselines we have confirmed that the signals are not intrinsic to the pulsar. These frequencies correspond to signals with periods; 5.55, 3.33, 2.38, and 1.11 ms. Since such values are close to the computed periods of several classes of neutron star oscillations (McDermott et al. 1988), these results serve to emphasize some of the difficulties encountered in searching for periodic signals in radio-pulsar data. Evidently, one must be cautious in drawing conclusions concerning the detection of periodicities in pulsar data which may contain contaminating signals.

5. DISCUSSION

Our results place several constraints on the neutron star oscillation hypothesis. First, if oscillations are somehow associated with the micropulse quasi-periodicities, then either the damping times of the relevant oscillations must be much less than the pulsar period, or else the magnetosphere must introduce substantial phase jitter, associated with variable emission radii or variable beaming angles. The former is what one would expect if the relevant oscillations were low-order p-modes, which are strongly damped by gravitational radiation
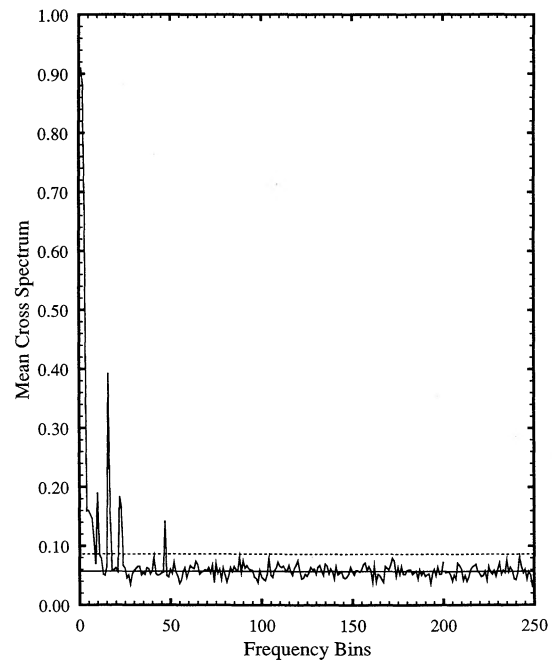

FIG. 9.—Plot of the mean of the $l = 1$–10 cross spectra computed from the last 250 pulses of our PSR 2016+28 data set. The four prominent peaks are due to harmonics of a 60 Hz signal which has contaminated the data set. From left to right, the signals correspond to the 3d, 5th, 7th, and 15th harmonics of the 60 Hz signal. The solid line denotes the mean value in the frequency range from bin 50 to 250. The dashed line is the corresponding 3 σ value in the same frequency range.

(McDermott et al. 1988). However, calculations of p-mode periods typically give values less than 0.2 ms for the lowest order modes, and the energy required to drive such oscillations to observable amplitudes are so large ($\approx 10^{47}$–10^{51} ergs) that there is no conceivable energy source capable of maintaining such oscillations. Alternatively, it is possible that the oscillations are "weakly" coupled to the radio emission mechanism, and therefore produce no apparent coherence of the microstructure; such a process might introduce phase jitter, as in our coherent micropulse simulations. Unfortunately, without a detailed theory of the pulsar magnetosphere and the radio emission mechanism it is impossible to be more precise about the nature of the coupling between the neutron star and the radio emission region. The success of the shot-noise models, including the random walk micropulse model, in reproducing the general features of the spectra of PSR 2016+28, as well as the low Q-value estimated for the micropulses, suggest that a chaotic or random process rather than a periodic one, perhaps in the magnetosphere itself, is responsible for the micropulse phenomena.

Second, the subpulse separation feature, P_2, which is easily detected in the auto spectrum, does exhibit significant coherence across several pulse periods. This suggests a higher Q-value for the process that produces the subpulse separation. Our model with variable subpulse drift reproduces many of the features seen in the auto and cross spectrum of PSR 2016+28. For this pulsar we characterize this process with a Q-value defined by $Q \equiv \text{(decay-time)/(period)} = 1.7 \times 0.53 \text{ s}/10 \text{ ms} \approx 90$. The drifting subpulse phenomenon has typically been explained in terms of drifting emission regions within the pulsar beam. The appearance of drifting subpulses in some pulsars and not others is then attributed to the orientation of the pulsar beam axis to the line of sight. Lines of sight which just graze the edges of the pulsar beam generally reveal drifting subpulses. This is reasonably consistent with the observation that most drifters show simple (unimodal) average pulse profiles (Backer 1976; Rankin 1983). This does not completely rule out a model based on stellar oscillation, however. An alternative interpretation is that the subpulse envelope is produced by an oscillation mode, and that the subpulse drift is simply the consequence of an incommensurate pulsar spin period and oscillation period. One difficulty with this interpretation is the apparent variation in drift rates which is seen in many pulsars. A possible explanation in the oscillation hypothesis is that the radio emission is not strongly coupled to the stellar oscillations, so that there is some phase jitter around the periodicity, similar to that in our variable drift rate simulations. This seems plausible in the circumstance that the radio emission is produced at some distance above the surface of the neutron star. Clearly, additional work is needed to decide this issue.

6. CONCLUSIONS

We have described a technique, based on analysis of the cross spectra of single-pulse data from pulsars, with which we can measure the coherence properties of, and search for coherent periodicities in, pulsar signals. To test our techniques and interpret results from actual pulsar data we have constructed and analyzed several simulated pulsar models. From an analysis of 2000 consecutive pulses from PSR 2016+28 we conclude: (1) the micropulse coherence time at 430 MHz is less than the spin period for this object. (2) This result could be consistent with a coherent model if the random phase jitter in such a model were $\geq 35\%$ of the micropulse quasi-periodicity. (3) The subpulse separation, $P_2 \approx 10$ ms, is coherent across 4–5 pulse periods, and is reasonably consistent with a model of subpulse drift that allows for variation about some mean drift rate. (4) A two-component (subpulse and micropulse) shot-noise model can reproduce much of the structure seen in the individual pulses as well as the spectra of PSR 2016+28.

REFERENCES

Arons, J. 1981, IAU Symp. 95, Pulsars, ed. W. Sieber & R. Wielebinski (Dordrecht: Reidel), 69
Asseim E., Pelletier, G., & Sol, H. 1990, MNRAS, 247, 529
Backer, D. C. 1973, ApJ, 182, 245
———. 1976, ApJ, 209, 895
Boriakoff, V. 1976, ApJ, 208, L43
Cordes, J. M. 1976a, ApJ, 208, 944
———. 1976b, ApJ, 210, 780
———. 1979, Space Sci. Rev., 24, 567
Cordes, J. M., Weisberg, J. M., & Hankins, T. H. 1990, AJ, 100, 1882
Hankins, T. H. 1971, ApJ, 169, 487
Jones, P. B. 1987, MNRAS, 228, 513
Kardashev, N. S., et al. 1978, AZh, 22, 583
McDermott, P. N. 1985, Ph.D. thesis, Univ. Rochester

McDermott, P. N., Van Horn, H. M., & Hansen, C. J. 1988, ApJ, 325, 725
Press, W. H., Flannery, B. P., Teukolsky, S. A., & Vetterling, W. T. 1986, Numerical Recipes (Cambridge: Cambridge Univ. Press)
Rankin, J. M. 1983, ApJ, 274, 333
———. 1986, ApJ, 301, 901
Rickett, B. J. 1975, ApJ, 197, 185
Soglasnov, V. A., Smirnova, T. V., Popov, M. V., & Kuz'min, A. D. 1981, AZh, 25, 442
Strohmayer, T. E. 1991, ApJ, 372, 573
Thorsett, S. E. 1990, private communication
Thorsett, S. E., & Stinebring, D. R. 1992, in IAU Coll. 128, The Magnetospheric Structure and Emission Mechanisms of Radio Pulsars, ed. T. Hankins, J. Rankin, & J. Gil (Dordrecht: Reidel), in press
Van Horn, H. M. 1980, ApJ, 236, 899